Structural and chemical disorder near the $Y_2BaCuO_5/YBa_2Cu_3O_{7-\delta}$ interface and its possible relation to the flux-pinning behavior in melt-textured $YBa_2Cu_3O_{7-\delta}$

Z. L. Wang,* A. Goyal, and D. M. Kroeger
Metals and Ceramics Division, Oak Ridge National Laboratory, P.O. Box 2008, Oak Ridge, Tennessee 37831
(Received 19 June 1992)

Transmission-electron microscopy and energy-dispersive x-ray spectroscopy were used to study the microstructure of the $YBa_2Cu_3O_{7-\delta}$ (1:2:3) region adjacent to the $Y_2BaCuO_5/YBa_2Cu_3O_{7-\delta}$ (2:1:1/1:2:3) interface. It is found that there exists a high local density of stacking faults in 1:2:3, near the 2:1:1/1:2:3 interfaces. The stacking faults lie parallel to the (001) basal plane and are inhomogeneously distributed around the 2:1:1 particles. They tend to be disk shaped with diameters ranging from a few to ~30 nm. Calculations made using simple energy considerations suggest that these stacking faults may act as effective flux pinners for magnetic fields directed both parallel and perpendicular to the basal plane. They may account for the observed increase of J_c with volume fraction of 2:1:1 and also explain the angular dependence of transport J_c in melt-processed 1:2:3. An unusual tendency for the formation of facets on the incoherent, randomly oriented 2:1:1 particles parallel to the {001}-type planes in the 1:2:3 matrix was also observed. Microanalysis of the 1:2:3 region around the 2:1:1 particles, which contain few or no stacking faults, consistently shows an enrichment of Y and a corresponding depletion in Ba concentration. Such cation nonstoichiometry may result in the formation of numerous point defects, which could also result in pinning. The presence of ledges on some facets at the 2:1:1/1:2:3 interfaces and the observed compositional nonstoichiometry in the 1:2:3 phase in the vicinity of these interfaces suggest that 2:1:1 particles continue to change in size after entrapment in 1:2:3. The observed compositional variation is consistent with dissolution of trapped 2:1:1. Such diffusion effects and stresses due to the thermal and elastic mismatch between 2:1:1 and 1:2:3 provide mechanisms for generating the observed defects aroung the 2:1:1 particles in the 1:2:3 matrix.

I. INTRODUCTION

The nature of microstructural features which are effective flux-pinning sites in highly anisotropic oxide superconductors is of considerable theoretical and technical interest. In the case of $YBa_2Cu_3O_{7-\delta}$ (1:2:3), a knowledge of flux-pinning mechanisms is needed to guide efforts to improve transport properties by processes which are consistent with the well-established need for an aligned microstructure, free of low J_c grain boundaries. The fabrication of highly aligned bulk 1:2:3 (Refs. 1-6) and 1:2:3/Ag (Refs. 5 and 6) composites with relatively few weakly linked boundaries has been accomplished. The microstructure within a single "domain" of aligned 1:2:3 and the growth mechanism of aligned 1:2:3 from the melt is now well understood.[7,8] One of the key microstructural features in melt-processed 1:2:3 is the existence of a random distribution of incoherent, ellipsoidal Y_2BaCuO_5 (2:1:1) particles trapped within the 1:2:3 phase due to an incomplete peritectic reaction.[1-8] It was found that during melt processing the presence of this network of 2:1:1 particles is essential for three-dimensional growth of 1:2:3.[7,8] 2:1:1 particles can also significantly affect the mechanical properties of aligned 1:2:3.[9,10] The presence of a random, incoherent distribution of trapped 2:1:1 particles within the aligned 1:2:3 matrix is analogous to a composite system composed of rigid particles in a brittle matrix.[10] The elastic and thermal anisotropy effects between the trapped 2:1:1 particles and the aligned 1:2:3 matrix in relation to the mechanical properties of 1:2:3 were discussed in a previous paper.[10] In such a composite system, defects can be expected to form at the interfacial regions between the two phases to accommodate the stresses produced after the imposed high-temperature processing cycle. There also exists an inherent chemical driving force for the dissolution of the trapped 2:1:1 particles. Such diffusive effects can also be expected to result in the formation of defect structures in the 1:2:3 matrix around 2:1:1 particles. Previous transmission electron microscopy (TEM) studies of melt-processed 1:2:3 indicate no significant change in the defect density near the 2:1:1/1:2:3 interface.[11] However, it was found from magnetization measurements that the critical current density J_c scales with the surface area of 2:1:1 trapped within the aligned 1:2:3 matrix, leading to the speculation that 2:1:1 particles act as flux-pinning sites.[12] Slight increases in the irreversibility lines were also observed.[12] Recent transport measurements on a single domain of aligned 1:2:3 with varying 2:1:1 content also show similar trends.[13] Since these trapped 2:1:1 particles are 2–3 orders of magnitude larger than the coherence length in 1:2:3, significant opposition to the view that they act as pinning sites has been expressed.[14,15] Remaining unexplained, however, is the important increase in the critical current density J_c with the surface area of 2:1:1 particles trapped within 1:2:3.

In order to get a better understanding of the above-stated problem, a detailed examination of the 2:1:1/1:2:3

interface was undertaken. The combined techniques of TEM and energy dispersion spectroscopy (EDS) were used to study the microstructure of the 1:2:3 region adjacent to the 2:1:1/1:2:3 interface. It is found that there exists a significant increase in the defect density in 1:2:3, near the 2:1:1/1:2:3 interface. Numerous stacking faults confined to the (001) basal plane are found in the 1:2:3 region adjacent to the 2:1:1 particles. Estimates indicate that the observed size and density of these stacking faults around the 2:1:1 particles may explain the observed increase of J_c with a volume fraction of 2:1:1.[12,13] The 1:2:3 region around the 2:1:1 particles also shows an enrichment of Y and a depletion of Ba relative to the stoichiometric composition. Such a cation nonstoichiometry may result in the formation of numerous point defects which could also result in additional flux pinning.

II. EXPERIMENT

The specimens used for this study were melt-textured thick films of 1:2:3 on a Ag 10% Pd alloy substrate. The films were prepared using a paint-on technique and processed according to a schedule reported elsewhere,[6,16] with a peak temperature of 1010 °C. Domains of 1:2:3, as large as 5–6 mm, are formed on the film. Figure 1 shows an optical micrograph of the cross section of the film. Normarski optical techniques show that a single 1:2:3 grain extends through the thickness of the film. The dark particles in the film have been identified by electron microprobe to be the 2:1:1 phase. Details of the microstructure-processing relations during the fabrication of aligned thick films of 1:2:3 are reported elsewhere.[16] It is important to note that careful microstructural examination of the film-substrate interface and grain boundaries intersecting this surface indicated that no significant reaction occurred between 1:2:3 and the substrate.

Analytical electron microscopy (AEM) studies of this material were made with a Philips EM400 TEM/STEM (100 kV) with a field emission gun (FEG). A small electron probe of diameter about 2 nm was generated and used in determining the compositional change across the grain boundary. The plan-view TEM specimens were prepared by grinding the substrate side and then ion milling to form thin foils. The specimen temperature was controlled to about −130 °C using a liquid-nitrogen double-tilt specimen holder during TEM examination. Almost no specimen damage and contamination were observed at 100 kV. The compositional variation was determined by manually scanning the electron probe across the 2:1:1/1:2:3 interface. It took about 2 min to acquire a single EDS spectrum. The electron-probe position was checked before and after EDS analysis to ensure there was no specimen drift. The distance of the probe from the interface was determined from the scanning transmission electron microscopy (STEM) image, and the position of the interface was located by the microdiffraction technique in STEM.

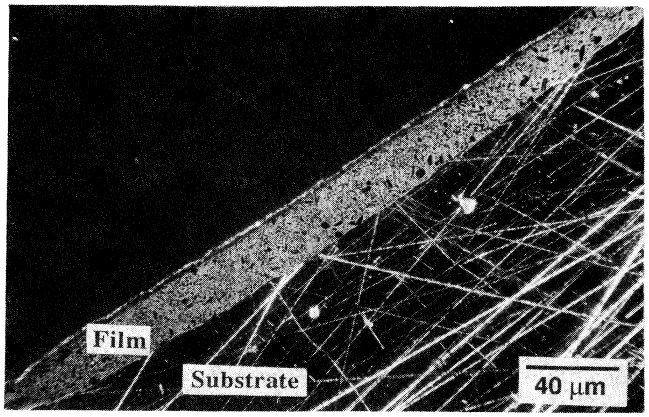

FIG. 1. Cross-section Normarski light micrograph of 1:2:3 thick film on a Ag 10% Pd substrate. Notice the clean interface between the film and the substrate. The micrograph is comprised of a single crystal of 1:2:3.

III. RESULTS AND DISCUSSION

A. 2:1:1/1:2:3 interface microstructure viewed along [100] or [010]

A melt-processed 1:2:3 grain usually contains many 2:1:1 particles. Figure 2(a) shows a typical low-magnification TEM image of 2:1:1 particles in a 1:2:3 grain. Figures 2(b) and 2(c) are enlargements of areas *b* and *c* indicated in Fig. 2(a). As seen in Fig. 2, the randomly oriented, incoherent 2:1:1 particles vary in size from 0.1 to 1.5 μm. The interface of 2:1:1 with 1:2:3 does not contain any amorphous material or even a third phase [Fig. 2(b)], and appears "clean." The existence of

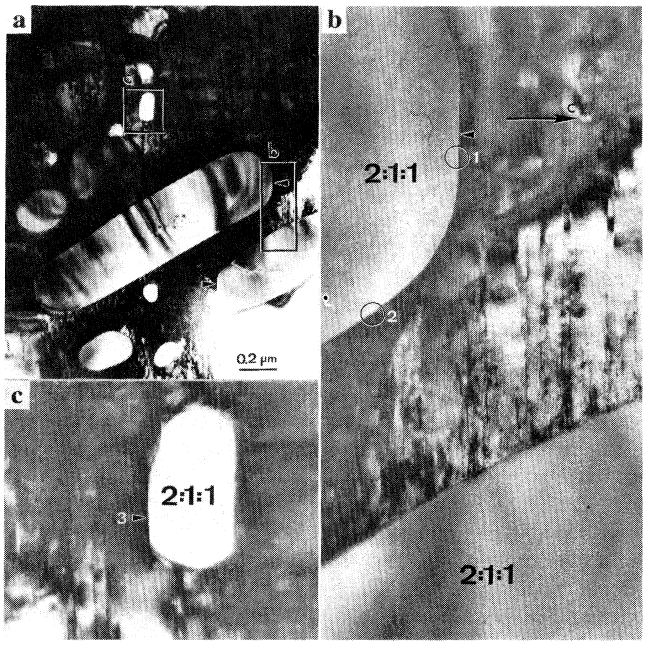

FIG. 2. TEM images of a melt-processes 1:2:3 material with 2:1:1 inclusions viewed along [100] or [010]. (b) and (c) are the enlarged areas *b* and *c* indicated in (a), respectively.

numerous stacking faults in the 1:2:3 matrix, adjacent to the 2:1:1/1:2:3 interface is apparent. Moreover, for some 2:1:1 particles, a facet is observed at the interface regions perpendicular to the c axis of the 1:2:3 matrix, as indicated by the arrow in Fig. 2. In some cases, the facets appear in pairs, bounding the two sides of the 2:1:1 particle [Fig. 2(c)]. However, facets were not seen on all 2:1:1 inclusions [Fig. 2(a)]. A ledge-type structure can sometimes be observed around the facet region as indicated by the arrow in Fig. 3. Relatively few stacking faults are observed in the 1:2:3 matrix around the facet region. The 2:1:1/1:2:3 interface region not perpendicular to the c axis of the 1:2:3 matrix usually shows a distinct curvature and contains more stacking faults.

The major defect structures seen in Figs. 2 and 3 are stacking faults in the ab plane. The nonuniform distribution of stacking faults around the 2:1:1 particle is an important indication of the strain inhomogeneity. This fact can be seen more clearly in Fig. 4. Interface areas perpendicular or nearly perpendicular to the c axis of 1:2:3 contain fewer stacking faults [Figs. 4(a) and 4(b)] than interface areas nearly parallel to the c axis of 1:2:3. In the latter areas the density of stacking faults is significantly higher than in the 1:2:3 matrix farther away from the particle [Fig. 4(c)].

The density of stacking faults around the 2:1:1 particle may depend on the local curvature of the particles with respect to the a-b planes. Figure 5 shows a comparison of two different 2:1:1 particle shapes. Although a facet is not observed in Fig. 5(a), the distribution of stacking faults is similar to that in Fig. 4. It is clear that the density of defects around the particle is much higher than that in the 1:2:3 matrix. Near a flat interface, as shown in Fig. 5(b), the density of defects is only slightly higher than that in the 1:2:3 matrix away from 2:1:1 surfaces. These observations show that the introduction of 2:1:1 inclusions definitely increases the density of stacking faults contained in the 1:2:3 matrix.

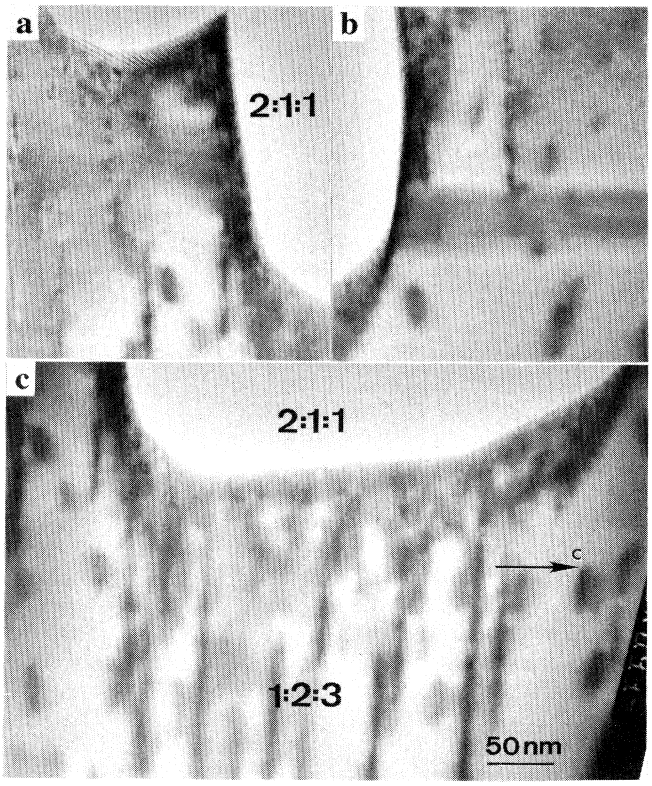

FIG. 4. (a)–(c) are TEM images from the left-hand, right-hand, and bottom sides of a 2:1:1 particle in the 1:2:3 matrix viewed along [100] or [010], respectively.

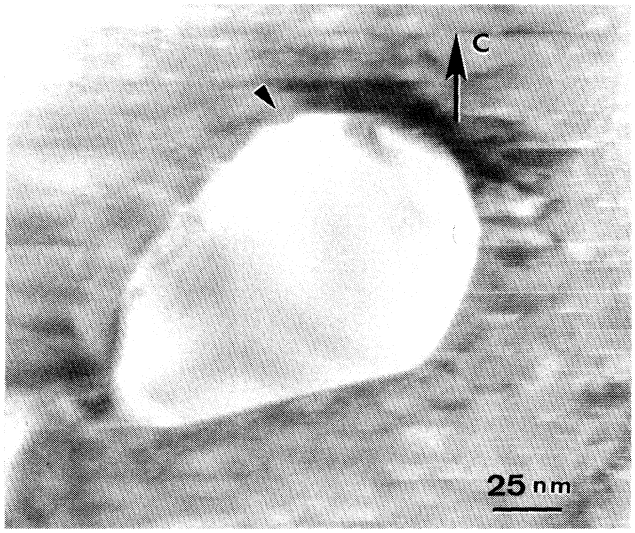

FIG. 3. A TEM image of a 2:1:1 particle in the 1:2:3 matrix viewed along [100] or [010] showing the facet and ledge types of structures at the interface region perpendicular to the c axis of 1:2:3.

B. 2:1:1/1:2:3 interface microstructure viewed along [001]

In order to further ascertain the association of stacking faults with individual 2:1:1 particles, examinations were made along the [001] zone axis. In this orientation, the

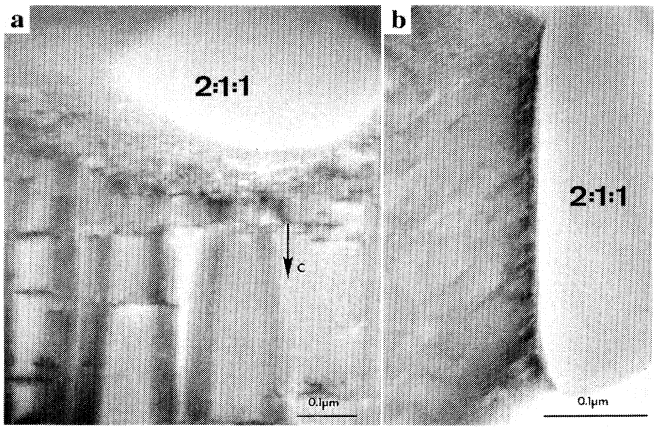

FIG. 5. TEM images of 2:1:1 inclusions in the 1:2:3 matrix viewed along [100] or [010] showing the high density distribution of stacking faults around the 2:1:1 particle interfaces.

strong dynamical scattering effect made it difficult to view along the exact zone axis. The specimen was thus tilted a few degrees off the [001] zone axis to form approximately the two-beam diffracting condition, so that the defect distribution could be more easily observed.

Besides the twin distribution, the only observed defect structures in this orientation are the small "precipitate"-like features which range in size from a few nm to 30 nm (Fig. 6). Similar to the stacking faults observed in Figs. 2–5, these clusters tend to distribute inhomogeneously around the 2:1:1 particles [Figs. 6(a) and 6(b)]. These clusters are probably small dislocation loops. Under the proper diffracting conditions, the $\mathbf{g}\cdot\mathbf{b}=0$ relationship is satisfied by some of the dislocations around the loop so that the loop is partly out of contrast along a line dividing the dark disk, as arrowed in Figs. 6(b) and 6(c). The out-of-contrast effect appears weak because the dislocation loop is quite small. The diameters of these dislocation loops are comparable to the lengths of the small stacking faults shown in Figs. 2–5. The convergent beam electron-diffraction (CBED) patterns taken from a dislocation loop [Fig. 7(a)] and the perfect 1:2:3 matrix [Fig. 7(b)] show two important characteristics. One is that the distributions of Bragg reflections for the two areas are the same. This indicates that the cluster is of the same crystallographic structure as 1:2:3. The other characteristic is that the Kikuchi pattern from the cluster [Fig. 7(a)] is split by a small angle, 2.5 mrad (0.14°), compared to that from 1:2:3 [Fig. 7(b)]. This is caused by the lattice distortion due to the presence of dislocations.

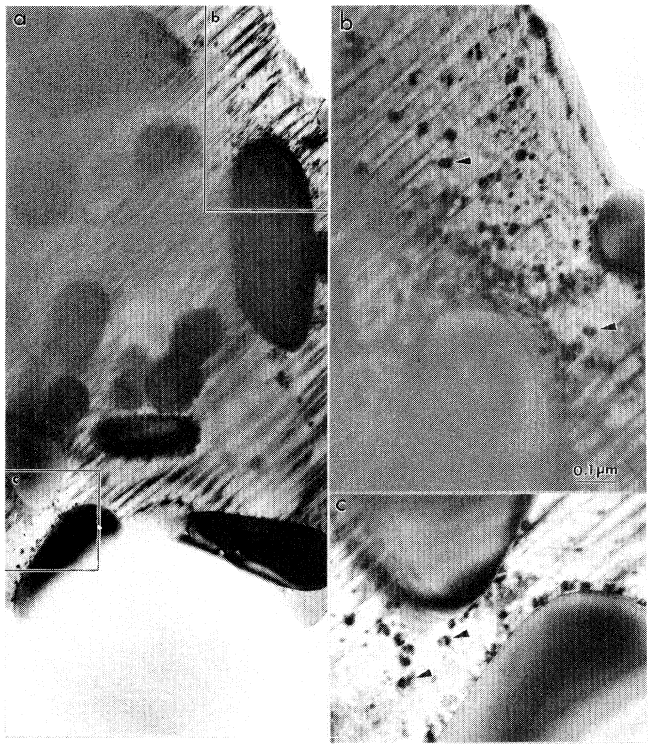

FIG. 6. TEM images of 2:1:1 inclusions in the 1:2:3 matrix viewed along [001]. (b) and (c) are enlarged images of the areas *b* and *c* indicated in (a) taken under slightly different diffracting conditions, respectively.

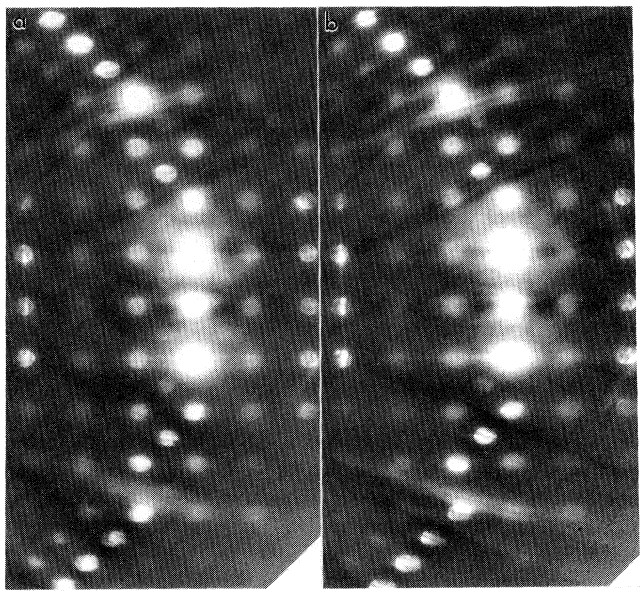

FIG. 7. (a) and (b) are CBED patterns taken using a 2-nm-diam electron probe from a dislocation loop and the 1:2:3 matrix, respectively.

These dislocation loops are probably associated with the stacking faults shown in Figs. 2–5. In the 1:2:3 matrix, the stacking fault structure may be produced by the introduction of an extra cation layer, which consequently disturbs the stacking sequences in 1:2:3. Strain at the periphery of this extra stacking layer is accommodated by a dislocation loop. When viewing along the [100]/[010] zone axis, some stacking faults appear to be longer than 30 nm. These are likely due to contrast from a few, overlapping, disk-shaped faults on the same basal plane, indicated in Figs. 6 and 8. Previous high-resolution transmission-electron microscopy (HRTEM) examinations in bulk and thin films of 1:2:3 have indicat-

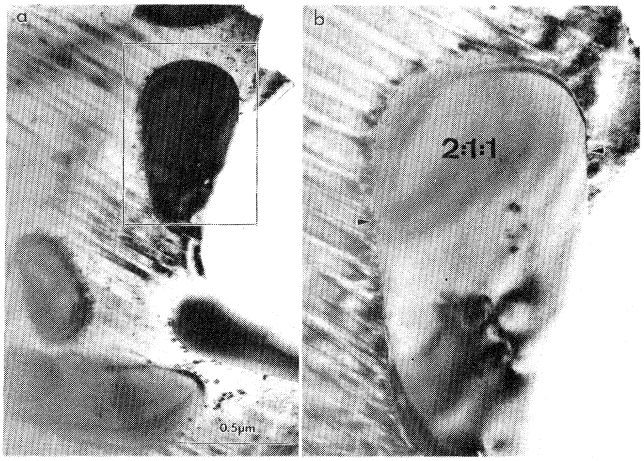

FIG. 8. TEM images of 2:1:1 inclusions in the 1:2:3 matrix viewed along [001]. (b) is an enlarged image of the area *b* indicated in (a) taken under slightly different diffracting conditions.

ed stacking faults corresponding to extra Cu, Y, and Ba oxide layers in the ideal 1:2:3 structure.[17–24] In each case the Burgers vector of the surrounding fault is not in the plane of the loop [i.e., is not in the (001) plane], but at some angle to it. The most commonly observed stacking fault in 1:2:3 corresponds to an intercalation of an extra CuO layer between the Ba layers. The partial dislocation bounding such a fault has a Burgers vector corresponding to $\pm 1/6(031)$. Such an extrinsic stacking fault of finite lateral extent, as observed here, is structurally analogous to a Frank loop in a typical fcc material. The dislocation surrounding such faults in the 1:2:3 phase is sessile in the (001) plane. Its slip plane corresponds to an inclined cylindrical surface defined by the Burgers vector and the dislocation line. The dislocation can, however, move in the plane of the loop by conservative and nonconservative climb mechanisms. At present, the nature of the stacking faults observed around the 2:1:1 particles is not known, i.e., whether they are Cu, Y, or Ba oxide layers. Hence, possible mechanisms which may result in the formation of these faults cannot be isolated. However, both compositional and stress-related effects can be expected to be operative.

Facets are sometimes also observed in this orientation. Figure 8 shows a low- and a high-magnification image of a trapped 2:1:1 particle. Faceting on one of the 2:1:1 particles is evident. The facet on the indicated particle is at 45° with the {110} twin plane, indicating it must be parallel to the (100) or (010) plane in the 1:2:3 matrix.

In summary, these observations suggest that the stacking faults are essentially disk-shaped regions and lie in the (001) plane. They vary in size from a few to ~30 nm in diameter.

C. Composition profiles across 2:1:1/1:2:3 interfaces

EDS analysis, using a 2-nm electron nanoprobe, was used to obtain information on the spatial compositional variation across the 2:1:1/1:2:3 interface. The electron probe was manually scanned across the interface and spectra were obtained at 5-nm intervals. A phase pure sample of aerosol-generated 2:1:1 powder was used as a standard to determine the k factors for microanalysis. Since the 2:1:1 phase is thought to be a strict line compound (in the Y-Ba-Cu-O system), it serves as an ideal standard for calibration. Figure 9(a) shows the atomic composition profile across the facet boundary indicated by 1 in Fig. 2(b). Considering the geometry of the partly embedded 2:1:1 particle within the 1:2:3 matrix in the specimen, the slow convergence of composition at the 2:1:1 side may indicate a large degree of 2:1:1 and 1:2:3 geometrical overlap along the beam direction. The composition at the 1:2:3 side converges quickly within about 10 nm because there is no overlap effect of 2:1:1 with 1:2:3 at this side. The composition of 1:2:3 at a distance 20 nm from the interface is ~1.15:1.85:3.0 (the composition is normalized to the ideal Cu content in 1:2:3), and at the interface is 1:1.1:1.4 (the composition at the 2:1:1/1:2:3 interface is normalized to Y, since under ideal conditions one would expect a composition of 1:1:1.33 at the interface). This indicates enrichment of yittrium in

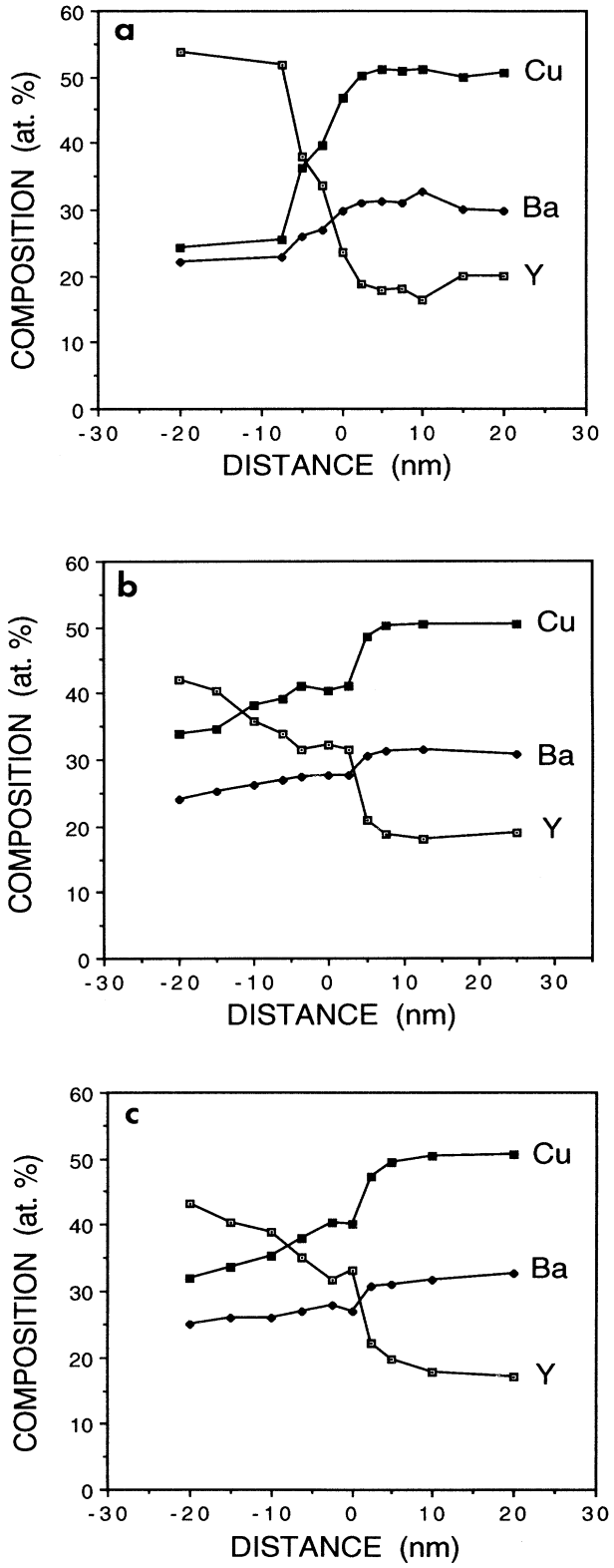

FIG. 9. (a) and (b) are composition profiles determined by EDS across the faceted (area 1) and nonfaceted (area 2) interface regions shown in Fig. 2(b) (see text for details). (c) A composition profile determined by EDS across the faceted interface region as indicated in Fig. 2(c).

the 1:2:3 matrix around the 2:1:1 particle. A compositional profile across the nonfaceted boundary indicated by 2 in Fig. 2(b) is shown in Fig. 9(b). As indicated in the figure, the composition of 1:2:3 20 nm away from the interface is ~1.2:1.9:3.0 and at the interface is 1:1.3:1.9. Again, a higher yittrium content is apparent. This also indicates that the interphase diffusion is about the same in the faceted and nonfaceted regions. In addition, the fast composition convergence at the 2:1:1 side in Fig. 9(b) may indicate that there is almost no geometrical overlap between 2:1:1 and 1:2:3 phases along the beam direction at area 2 in Fig. 2(b). A compositional scan across a faceted interface on a smaller 2:1:1 particle as indicated in Fig. 2(c) is shown in Fig. 9(c). The composition at a distance 20 nm from the interface is ~1:2:3, and at the interface is ~1:1.2:1.4. Across this interface the composition of 1:2:3 reaches a stoichiometric value at a short distance of ~5–6 nm. The composition at the interface of 2:1:1/1:2:3 can be expected to be an average composition between 2:1:1 and 1:2:3, i.e., ~1:1:1.33. This is close to what is observed in all cases [Figs. 9(a)–9(c)]. Small deviations from this ideal composition at the interface are inconclusive since the beam may be slightly off centered from the interface.

D. Mechanisms for formation of defects in 1:2:3 near 2:1:1/1:2:3 interfaces

The physical processes dominating the formation of defects in 1:2:3 at the vicinity of 2:1:1 particles cannot be isolated from this study. However, as discussed previously, both stress-related (because of the thermal expansion and elastic modulus mismatch[10]) and chemical effects due to the inherent tendency for dissolution of trapped 2:1:1 can be expected to be operative. Besides the high density of stacking faults and cation nonstoichiometry in 1:2:3 near 2:1:1 particles, another distinctive microstructural feature is the formation of facets at 2:1:1/1:2:3 interfaces. Mechanisms resulting in the formation of facets may be closely linked to those resulting in the formation of defects in 1:2:3.

As noted before, facets form only at some 2:1:1/1:2:3 interfaces, and they always terminate with a {001}-type plane in 1:2:3. These facets could be formed during encasement of 2:1:1 particles at the growth front or after prior encasement. Anisotropic growth of 1:2:3 may explain the formation of facets with the (001) plane in 1:2:3, but not with the (010) or (100) planes, and hence the latter possibility seems more likely. Formation of facets after prior encasement of 2:1:1 would be dictated by interfacial energy effects. However, since the 2:1:1 particles are randomly oriented within the aligned 1:2:3 matrix, and the facets always tend to terminate with a {001}-type plane in 1:2:3, facet formation appears to be dominated by the anisotropic surface energies in 1:2:3. It is well established that {001}-type planes in 1:2:3 have the lowest surface energy, and that the surface energy of the (001) plane is lower than both the (100) and (010) planes.[9]

Surface energy effects can result in the formation of facets by either a rearrangement of the 2:1:1 particle, i.e., a change in shape of the particle, or by local growth of 1:2:3, i.e., a change in size of the particle. Rearrangement of the 2:1:1 particle to form facets would require significant displacement of atoms both in the 1:2:3 and the 2:1:1 phases. The 2:1:1/1:2:3 interface provides an easy channel for diffusion of atoms in both directions. However, since facets are formed only on some of the 2:1:1 particles, with no apparent size or orientation dependence, this may not be the sole mechanism for facet formation. Local growth of 1:2:3 near 2:1:1 particles and the influence of surface energies in 1:2:3 can result in the formation of facets. The presence of ledges on some facets provides evidence for growth of 1:2:3. Local growth of 1:2:3 does not necessarily require long-range diffusion, since the close proximity of platelet boundaries with some 2:1:1 particles provides an ample supply of Ba- and Cu-rich phases.[7,8] However, conversion of 2:1:1 to 1:2:3 is accompanied by a significant volume change. It can easily be shown that for a 2:1:1 particle of volume V, if only 36 vol. % of 2:1:1 reacts peritectically with Ba- and Cu-rich phases, it will form 1:2:3 of volume V. This large volume change accompanying the transformation of 2:1:1 to 1:2:3, and the absence of voids or cracks at the 2:1:1/1:2:3 interfaces, suggests that for any conversion to occur, a significant amount of yttrium must also diffuse away from the 2:1:1/1:2:3 interface into the surrounding 1:2:3 matrix. This may provide a mechanism for the observed yttrium enrichment near the 2:1:1 particles. The yttrium enrichment near the 2:1:1 particles could, however, be quenched-in cation disorder from high temperatures.

Formation of stacking faults is also expected to be linked to both chemical and stress-related effects. Diffusive effects relating to growth of 1:2:3 may result in stacking faults. The thermal expansion and elastic modulus mismatch between 2:1:1 and 1:2:3 provides a driving force for the formation of stacking faults near the 2:1:1/1:2:3 interfaces. Since 1:2:3 contracts much more than 2:1:1 along the c direction, the 1:2:3 region near the 2:1:1 particle is put in a state of tension. One way to relieve such stresses without forming cracks or voids, is by the formation of numerous stacking faults at 2:1:1/1:2:3 interfaces. It is important to note that the lattice fringes of 1:2:3 close to the 2:1:1 particles appear to be stress free. Further understanding of mechanisms for formation of the observed stacking faults will result from identification of their chemical nature and the Burgers vector of the dislocation surrounding these faults. This is currently in progress.

E. Microstructure of other melt-processed samples

In order to ascertain if similar microstructures are present in samples processed using different schedules, several other specimens are currently being examined. In particular are bulk specimens processed using the standard melt process[3–6] and specimens processed according to the quench-melt-growth (QMG) technique of Murakami *et al.*[12] It is found that a similar microstructure is present in all specimens irrespective of the processing technique. Specimens processed using the QMG technique appear to have an even higher local density of

stacking faults per unit volume than that reported here.[25] Details of microstructural examinations on these samples will be reported elsewhere.

F. Stacking faults as pinning sites

The numerous stacking faults observed around 2:1:1 particles and defect structures associated with them have dimensions which are appropriate for flux pinning. The stacking faults around the 2:1:1 particles can be viewed as disks of additional material with diameters ranging from a few to ~30 nm. The nature of the dislocations bounding these stacking faults will dictate their pinning characteristics. As discussed in a previous section, the dislocation loops can be expected to have a Burgers vector inclined at an angle to the plane of the loop. HREM studies by Marshall *et al.*[24] have shown that for CuO stacking faults, the (001) lattice fringes in the vicinity of the dislocation loop bounding the fault are bent to accommodate the extra plane of atoms. Depending on the lateral extent of the fault, the strain generated may extend up to 3 unit cells above and below the plane of the fault.[24] Hence, for $H \| c$, small stacking faults (a few nm in diameter), may act as point pins. For large faults (~30 nm), pinning of the flux lines would occur primarily at the circumferential region defined by the dislocation loop bounding the fault. The strength of pinning would depend on the length of the flux line that is pinned, and in this case that may correspond to the extent of crystal lattice strain along the c direction. For $H \| ab$, the length of the flux line pinned is equivalent to the dimension of the fault in the basal plane. The strain field in the crystal around the stacking fault does not significantly change the effective length of the flux line pinned in this orientation, since the lattice parameter is small in the basal plane (assuming the strain field extends to only 3 unit cells around the fault in the ab plane).

Flux pinning due to stacking faults can be ascribed to the local disruption of the 1:2:3 crystal lattice where the condensation energy is decreased. Hence, the energy cost of locating a flux line in this region is reduced. The system effectively gains the pinning energy $U_p = \eta(H_c^2/8\pi)\nu$, where $\eta < 1$, is the fractional suppression of superconductivity in the defect, H_c is the thermodynamic critical field, and ν is the volume of the vortex core that is pinned.[26,27] For $H \| c$, the volume of the vortex core pinned is $\nu = \pi\xi_{ab}^2 L$, where ξ_{ab} is the Ginzburg-Landau coherence length in the ab plane and L is either $2\xi_c$ (ξ_c is the Ginzburg-Landau coherence length in the c direction) or the distance along the c direction affected by strain due the presence of the stacking fault. The elementary pinning force f_p is given by $f_p \sim U_p/2\xi_{ab}$, since the Lorentz force is directed along the ab plane in this field orientation. Assuming direct summation of pinning forces, the maximum bulk-pinning force F_p is given by $F_p = N_p f_p$, N_p being the number density of pinning centers per unit volume. Also, $F_p = J_c B/10$ (F_p is in dyne/cm^3, J_c in A/cm^2, and B in Oe). Hence $J_c = 5N_p f_p/B = 5N_p \eta H_c^2 \xi_{ab} L/8B$.

For $H \| ab$, the volume of the vortex core that is pinned is $\nu = \pi\xi_{ab}\xi_c d$, d being the length of the stacking fault in the direction of the field. For this field orientation the Lorentz force is directed perpendicular to the basal plane, so that the pinning force $f_p \sim U_p/2\xi_c$. Hence $J_c = 5N_p \eta H_c^2 \xi_{ab} d/8B$.

To calculate the critical current density arising from flux pinning by stacking faults, an estimate for their density is required. The stacking fault density can be estimated by a number of methods, and a conservative estimate was found to be $\sim 10^{15}$/cm^3. For example, the density can be calculated using the 2:1:1 particle shown in Fig. 6(b). The particle can be approximated by a cylinder, 0.2 μm in diameter and 0.5 μm long. The thickness of the TEM foil is estimated to be ~100 nm. Assuming that the 2:1:1 particle extends through the thickness of the foil, and that every stacking fault in the foil around the particle is imaged under the diffraction conditions used in Fig. 8, the stacking fault density per unit surface area of the 2:1:1 particles can be calculated. The number of individually distinguishable loops around the particle is estimated to be ~70. The surface area of the 2:1:1 particle contributing to these stacking faults is defined by the perimeter of the particle times the thickness of the foil, and is estimated to be 1.4×10^{-9} cm^2. Hence the stacking fault density per unit surface area of 2:1:1 is calculated to be $\sim 5 \times 10^{10}$ faults/cm^2. The area/volume ratio of a cylindrical particle is $2/r + 2/h$, where r and h are the radius and length of the particle, respectively. Assuming an average 2:1:1 particle size to be 0.5 μm by 1 μm, and the volume fraction of trapped 2:1:1 to be 0.2, the overall stacking fault density is calculated to be $\sim 10^{15}$/cm^3. The stacking fault density estimated by other methods using the images of Figs. 2–8 is found to be higher than 10^{15}/cm^3.

Using the experimentally deduced values of ξ_{ab}, ξ_c, and H_c at 4.2 and 77 K, as determined by Ossandon[28] and indicated in Table I, and assuming $\eta = 1$, we have the following estimates for the critical current density.

For $H \| c$: A low estimate for the critical current density can be obtained by assuming there is no strain in the crystal around the stacking fault or $L = 2\xi_c$, this gives

$$J_c \sim 10^5 \text{ A/cm}^2 \text{ at } 4.2 \text{ K and } 1 \text{ T}$$
$$\sim 10^4 \text{ A/cm}^2 \text{ at } 77 \text{ K and } 1 \text{ T} .$$

A higher estimate for the critical current density can be obtained by assuming that the maximum extent of strain field around the stacking fault in the c direction is 3 unit cells above and below the plane of the fault,[24] i.e., $L \sim 6$ unit cells ~70 Å, this gives

$$J_c \sim 10^6 \text{ A/cm}^2 \text{ at } 4.2 \text{ K and } 1 \text{ T}$$
$$\sim 10^5 \text{ A/cm}^2 \text{ at } 77 \text{ K and } 1 \text{ T} .$$

TABLE I. Experimentally deduced values of ξ_{ab}, ξ_c, and H_c (Ref. 28).

	4.2 K	77 K
ξ_c	2.85 Å	6.5 Å
ξ_{ab}	15.4 Å	35 Å
H_c	10.65 kG	1.73 kG

These values compare very well with those observed experimentally.[12,13] In samples with nominally higher Y or 2:1:1 contents, J_c values can be expected to scale with increase in the 2:1:1/1:2:3 interfacial area.

For $H \| ab$: Assuming the average diameter, d, of the stacking faults to be 10 nm,

$$J_c \sim 10^6 \text{ A/cm}^2 \text{ at 4.2 K and 1 T}$$

$$\sim 10^5 \text{ A/cm}^2 \text{ at 77 K and 1 T .}$$

As mentioned before, in this orientation the effect of crystal strain does not significantly change the length of the flux line that is pinned. Moreover, since the lattice strain can extend up to ~ 3 unit cells ~ 35 Å on either side of the fault in the c direction, and since the coherence length along the c direction is much smaller than this dimension, the presence of lattice strain may not be beneficial, since the Lorentz force is directed in the c direction. This should be especially true at low temperatures since the coherence length is considerably reduced, as indicated in Table I. In any case, intrinsic pinning probably overshadows the estimated contribution to J_c from stacking faults in this field orientation.

Flux decoration experiments involving ferromagnetic Ni particles,[29] the Faraday effect of an iron garnet film,[29] and ferromagnetic Fe particles[30] clearly show that at low flux densities, the fluxoids are inhomogeneously pinned at the 2:1:1/1:2:3 interfaces. The inhomogeneous distribution of stacking faults around the 2:1:1 particles as observed here correlates well with the distribution of flux lines indicated by these experiments.

The transport critical current density of bulk melt-processed 1:2:3 shows a considerable anisotropy in the presence of a magnetic field.[13,31,32] Two peaks in the transport J_c were found when the angle θ between the direction of applied magnetic field and the c axis was varied. One narrow peak located at $H \| ab$ is related to intrinsic pinning by the anisotropic crystal structure. Another peak, the origin of which was not understood, was observed at $H \| c$.[13,31,32] Flux pinning by stacking faults around trapped 2:1:1 particles may explain this peak.

G. Flux pinning by other defects

Other potential pinning sites in melt-processed 1:2:3 include twin planes and point defects. Pinning by twin planes has been demonstrated to be weak and is effective only at low fields which are well aligned with the twin planes, such that the Lorentz force is directed perpendicular to the twin planes.[33–37] Increasing the twin density in melt-processed 1:2:3 has little effect on J_c and so twin planes are not a dominant pinning site.[38,39] However, certain kinds of point defects may be effective pinning sites. Since 2:1:1 particles continue to dissolve by converting to 1:2:3, numerous point defects must be created around these particles. In fact, a simple calculation shows that for $x = 0.1$ in the system $Y_{1+x}Ba_{2-x}Cu_3O_{7-\delta}$, this corresponds to a point defect density of $\sim 10^{19}/\text{cm}^3$. As mentioned previously, the 1:2:3 matrix at the vicinity of the particle interface is Y rich and Ba poor. It is possible that point defects resulting from the solid-state diffusion of yttrium away from these particles may contribute to pinning. Point defects created in such a manner can be expected to be different in nature from those created by oxygen deficiency. It is, however, important to note that recent investigations of substitutions by trivalent rare-earth Nd atoms on divalent Ba sites in the $Nd_{1+x}Ba_{2-x}Cu_3O_{7-\delta}$ system have shown that the mobile hole concentration in the CuO_2 planes changes with x, in a manner similar to the variation of T_c with x.[40] This is analogous to the situation in $YBa_2Cu_3O_{7-\delta}$ where the primary effect of vacancies on the chain sites is also to modify the mobile charge carrier density in the CuO_2 planes.[41] Ossandon *et al.*[28] and Christen *et al.*[42] have found from magnetization and transport measurements in 1:2:3 that J_c decreases with increasing oxygen vacancy concentration, even in the 90-K plateau of the T_c versus δ curve, i.e., for $\delta < 0.2$, and conclude that the dominant effect on J_c is the decrease in carrier density. The effectiveness of flux pinning by point defects created by substitution of Y on the Ba sites in the $Y_{1+x}Ba_{2-x}Cu_3O_{7-\delta}$ system is yet to be determined. It is important to note that despite the observed cation nonstoichiometry around the 2:1:1 particles, no reduction in the transition temperature is found. A sharp transition at 91 K is a common feature of melt-processed 1:2:3.

Flux pinning by point defects in general is controversial, even in the case of irradiated 1:2:3. This is because the nature of defects created by various kinds of irradiation has not been completely characterized and it is difficult to separate the contribution from different defects in the sample. Both neutron and proton irradiation result in enhanced critical currents, however, little effect is observed on the irreversibility lines of 1:2:3.[43–45] Neutron irradiation is believed to result in some kind of a microcellular structure consisting of 5–10-nm regions of nonsuperconducting material embedded in good superconducting material.[43,44] These nonsuperconducting regions are thought to be responsible for pinning. TEM observations of proton irradiated single crystals of 1:2:3 indicate the presence of small clusters about 3 nm in size and spaced about 30 nm.[44] In both cases, it is not clear whether the dominant contribution to pinning is from these large observed clusters or a possible array of background point defects which are difficult to detect in the electron microscope. Unfortunately, no compositional scans were made in regions of ordered 1:2:3, and hence there is even no indirect evidence which shows that some point defects were generated. Electron irradiation which presumably does result in the generation of numerous point defects does not result in enhanced pinning.[45,46] However, in this case, the maximum atom displacements are produced in the oxygen sublattice,[46] point defects which have been shown not to be effective pinning sites.[28] Hence, the pinning effectiveness of point defects around the 2:1:1 particles remains an open question.

IV. CONCLUSIONS

Detailed microstructural examination of 2:1:1/1:2:3 interfaces in melt-processed 1:2:3 using TEM indicates a

high local density of stacking faults ($> 10^{15}/cm^3$) in 1:2:3 near the 2:1:1/1:2:3 interfaces. The stacking faults lie parallel to the (001) plane and are inhomogeneously distributed around the 2:1:1 particles. TEM examinations with the beam directed approximately along the [001] zone axis indicate that these stacking faults are disk shaped with diameters ranging from a few to ~30 nm. The dislocation loops bounding the stacking faults are visible in this orientation.

An unusual tendency for the formation of facets on the incoherent, randomly oriented 2:1:1 particles with the {001}-type planes in 1:2:3 was also observed. No preferential orientation in the 2:1:1 particle with respect to the facet was observed. Surface energy considerations are believed to have a dominant role in the formation of these facets along the low surface energy {001}-type planes in 1:2:3. Ledges were sometimes also observed on the 2:1:1 particles.

EDS analysis, using a 2-nm electron nanoprobe, was used to get information on the spatial compositional variation in the 1:2:3 phase near the 2:1:1/1:2:3 interfaces, where little or no stacking faults were present. It is found that there is a considerable enrichment in Y and a depletion in Ba in the 1:2:3 matrix around the 2:1:1 particle. Such cation nonstoichiometry may result in the formation of numerous point defects in 1:2:3 around the 2:1:1 particles. The presence of these facets, ledges on some facets, and the observed compositional disorder around the 2:1:1 particles suggests that 2:1:1 particles change in size after entrapment in 1:2:3. The observed compositional variation is consistent with the dissolution of 2:1:1.

The numerous stacking faults around the 2:1:1 particles and defect structures associated with them have dimensions which are appropriate for flux pinning. For $H \| c$, small stacking faults (a few nm) can act as point pins. For large stacking faults (~30 nm), pinning can be expected to occur primarily at the circumferential region defined by the dislocation loop bounding the fault. The strength of pinning would depend on the extent of crystal lattice strain along the c direction. For $H \| ab$, the length of the flux line pinned is equivalent to the dimension of the fault in the basal plane. Calculations of the critical current density made using simple energy considerations agree very well with the experimentally measured values, suggesting that these stacking faults may be effective pinning centers. They may account for the observed increase in J_c with a surface area of 2:1:1, and the angular dependence of transport J_c in melt-processed 1:2:3, namely, the peak in J_c for $H \| c$. The creation of numerous cation-related point defects in the 1:2:3 matrix around the 2:1:1 particles may also provide additional background pinning.

ACKNOWLEDGMENTS

We thank Dr. D. K. Christen and Dr. K. B. Alexander for comments. The research was supported by the U. S. Department of Energy, Office of Advanced Utility Concepts-Superconducting Technology Program, under Contract No. DE-AC05-84OR21400 with Martin Marietta Energy Systems, Inc.

*Also at Department of Materials Science and Engineering, The University of Tennessee, Knoxville, TN 37996-2200.

[1]S. Jin, T. H. Tiefel, R. C. Sherwood, R. V. van Dover, M. E. Davis, G. W. Kammlott, and R. A. Fastnacht, Phys. Rev. B **37**, 7850 (1988).

[2]M. Murakami, M. Morita, K. Doi, and K. Miyamoto, Jpn. J. Appl. Phys. **28**, 1189 (1989).

[3]K. Salama, V. Selvamanickan, L. Gao, and K. Sun, App. Phys. Lett. **54**, 2353 (1989).

[4]P. J. McGinn, W. Chen, N. Zhu, U. Balachandran, and M. T. Lanagan, Physica C **165**, 480 (1990).

[5]A. Goyal, Ph.D. thesis, University of Rochester, 1991; A. Goyal, P. D. Funkenbusch, and S. J. Burns (unpublished).

[6]A. Goyal, P. D. Funkenbusch, D. M. Kroeger, and S. J. Burns, Physica C **182**, 203 (1991).

[7]K. B. Alexander, A. Goyal, D. M. Kroeger, V. Selvamanickam, and K. Salama, Phys. Rev. B **46**, 5622 (1992).

[8]A. Goyal, K. B. Alexander, D. M. Kroeger, P. D. Funkenbusch, and S. J. Burns (unpublished).

[9]A. Goyal, P. D. Funkenbusch, D. M. Kroeger, and S. J. Burns, J. Appl. Phys. **71**, 2363 (1991).

[10]A. Goyal, W. C. Oliver, P. D. Funkenbusch, D. M. Kroeger, and S. J. Burns, Physica C **183**, 221 (1991).

[11]K. Yamaguchi, M. Murakami, H. Fujimoto, S. Gotoh, T. Oyama, Y. Shiohara, N. Koshizuka, and S. Tanaka, J. Mater. Res. **6**, 1404 (1991).

[12]M. Murakami, S. Gotoh, N. Koshizuka, S. Tanaka, T. Matsuhita, S. Kanube, and K. Kitazawa, Cryogenics **30**, 390 (1990).

[13]K. Salama, D. F. Lee, and X. Chaud (unpublished).

[14]S. Jin, T. H. Tiefel, and G. W. Kamlott, Appl. Phys. Lett. **59**, 540 (1991).

[15]P. McGinn, N. Zhu, W. Chen, S. Sengupta, and T. Li, Physica C **176**, 203 (1991).

[16]A. Goyal *et al.* (unpublished).

[17]H. W. Zandbergen, R. Gronsky, and G. Thomas, Phys. Status Solidi A **105**, 207 (1988).

[18]J. Tafto, M. Suenaga, and R. L. Sabatine, Appl. Phys. Lett. **52**, 667 (1988).

[19]M. J. Kramer, L. S. Chumbley, R. W. McCallum, W. J. Nellis, S. Wier, and E. P. Kvam, Physica C **166**, 115 (1990).

[20]S. T. Weir, W. J. Nellis, M. J. Kramer, S. L. Seamen, E. A. Early, and M. B. Maple, Appl. Phys. Lett. **56**, 2042 (1990).

[21]J. Kulik, J. Appl. Phys. **70**, 4398 (1991).

[22]D. J. Li, Shibahara, J. P. Zhang, L. D. Marks, H. O. Marcy, and S. Song, Physica C **156**, 201 (1988).

[23]D. Dominges, M. Herview, C. Micheal, and B. Raveau, Europhys. Lett. **4**, 211 (1987).

[24]A. F. Marshall, K. Char, R. W. Barton, A. Kapitulnik, and S. S. Laderman, J. Mater. Res. **5**, 2049 (1990).

[25]Z. L. Wang, A. Goyal, D. M. Kroeger, and T. Armstrong, in *Layered Superconductors: Fabrication, Properties and Applications, MRS* Symposia Proceedings No. 275, edited by D. T. Shaw, C. C. Tsuei, T. R. Schneider, and Y. Shioshara (Materials Research Society, Pittsburgh, 1992), p. 181.

[26]P. W. Anderson, Phys. Rev. Lett. **9**, 309 (1962).

[27]A. M. Campbell and J. E. Evetts, Adv. Phys. **21**, 199 (1972).

[28]J. G. Ossandon, Ph.D. thesis, University of Tennessee, 1991; J.

G. Ossandon *et al.*, Phys. Rev. B **46**, 3050 (1992).
[29]M. Murakami, H. Fujimoto, S. Gotoh, K. Yamaguchi, N. Koshizuka, and S. Tanaka, Physica C **185-189**, 321 (1991).
[30]L. Tong, H. Chen, G. Wang, S. Yan, C. Zhang, H. Zhang, J. Xu, H. Ren, L. Xiao, and Q. He, Solid State Commun. **76**, 341 (1990).
[31]D. K. Christen, C. E. Klabulnde, M. J. Neal, M. V. Parish, D. B. Chandler, B. C. Chakoumakos, A. Goyal, and D. M. Kroeger (unpublished).
[32]J. W. Ekin, K. Salama, and V. Selvamanickam, Appl. Phys. Lett. **59**, 360 (1991).
[33]T. R. Dinger, G. J. Golan, D. Keane, T. R. McGuire, T. K. Wirthington, R. M. Yandrofski, and Y. Yeshrun, in *High-Temperature Superconductors,* edited by S. H. Whang and A. DasGupta (The Minerals, Metals & Materials Society, Chicago, 1989), p. 23.
[34]V. V. Moshchalkov, O. V. Petrenko, A. A. Zhukov, A. A. Gippus, V. I. Voronkova, V. S. Belov, and V. A. Rybachuk, Phys. C **162-164**, 1611 (1989).
[35]L. J. Swartzendruber, D. L. Kaiser, F. W. Gayle, L. H. Bennett, and A. Roytburd, Appl. Phys. Lett. **58**, 1566 (1991).
[36]W. Kritscha, F. M. Sauerzopf, H. W. Weber, G. W. Crabtree, and J. Z. Liu, Supercond. Sci. Technol. **4**, S259 (1991).
[37]W. K. Kwok, U. Welp, G. W. Crabtree, K. G. Vandervoort, R. Hulscher, and J. Z. Liu, Phys. Rev. Lett. **64**, 966 (1990).
[38]V. Selvamanickan, Ph.D. thesis, Department of Mechanical Engineering, University of Texas, Houston (1992).
[39]D. K. Christen and R. Feenstra, Physica C **185-89**, 2225 (1991); R. Feenstra, D. K. Christen, C. E. Klabunde, and J. D. Budai, Phys. Rev. B **45**, 7555 (1992).
[40]K. Takita, H. Akinaga, T. Ohshima, Y. Takeda, and M. Takano, Physica C **191**, 509 (1992).
[41]R. J. Cava, A. W. Hewat, E. A. Hewat, B. Battlogg, M. Marezio, K. M. Rabe, J. J. Krajewski, W. F. Peck, Jr., and L. W. Rupp, Jr., Physica C **165**, 419 (1990).
[42]H. W. Weber, H. P. Wiesinger, W. Kritscha, and F. M. Saurzopf, Supercond. Sci. Technol. **4**, S103 (1991).
[43]M. A. Kirk, M. C. Frishher, J. Z. Liu, L. R. Greenwood, and H. W. Weber, Philos. Mag. Lett. **62**, 41 (1990).
[44]L. Civale, A. D. Marwick, M. W. McElfresh, T. K. Worthington, A. P. Malozemoff, F. H. Holtzberg, J. R. Thompson, and M. A. Kirk, Phys. Rev. Lett. **65**, 1164 (1990).
[45]M. Konczykowski, F. Rullier-Albenque, Y. Yeshrun, E. R. Yacoby, A. Shaulov, and J. Gilchrist, Supercond. Sci. Technol. **4**, S445 (1991).
[46]H. Vicery, F. Rullier-Albenque, H. Pascard, M. Konczykowski, R. Kormann, D. Favrot, and G. Collin, Physica C **159**, 697 (1989).

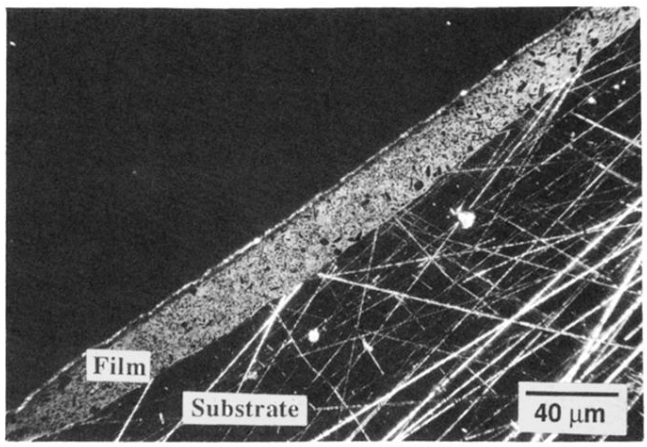

FIG. 1. Cross-section Normarski light micrograph of 1:2:3 thick film on a Ag 10% Pd substrate. Notice the clean interface between the film and the substrate. The micrograph is comprised of a single crystal of 1:2:3.

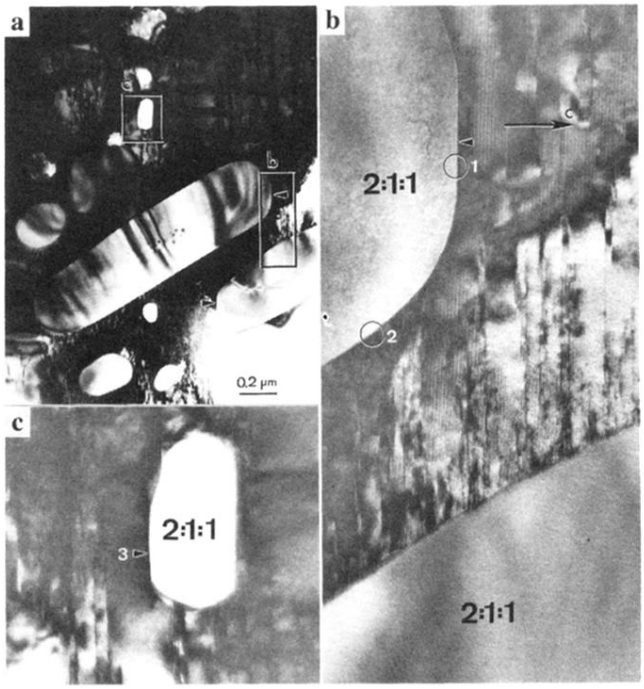

FIG. 2. TEM images of a melt-processes 1:2:3 material with 2:1:1 inclusions viewed along [100] or [010]. (b) and (c) are the enlarged areas *b* and *c* indicated in (a), respectively.

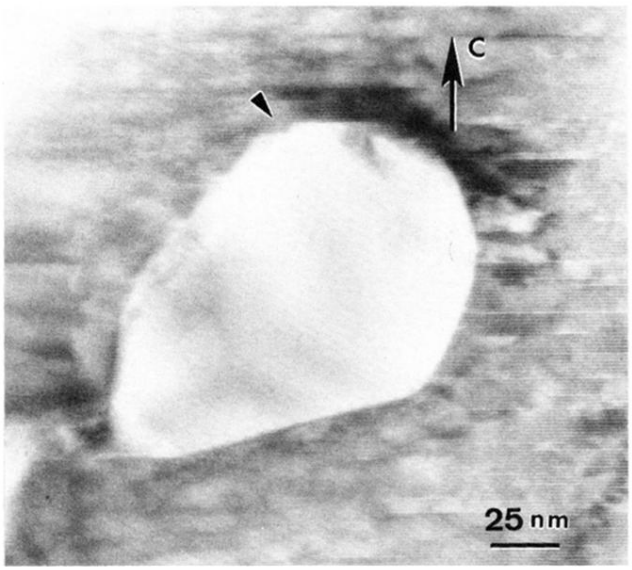

FIG. 3. A TEM image of a 2:1:1 particle in the 1:2:3 matrix viewed along [100] or [010] showing the facet and ledge types of structures at the interface region perpendicular to the *c* axis of 1:2:3.

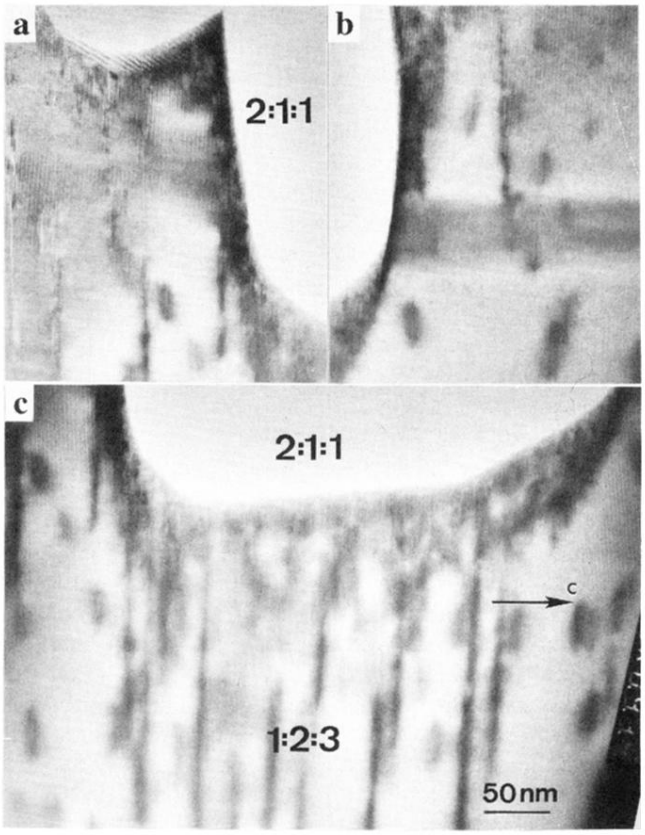

FIG. 4. (a)–(c) are TEM images from the left-hand, right-hand, and bottom sides of a 2:1:1 particle in the 1:2:3 matrix viewed along [100] or [010], respectively.

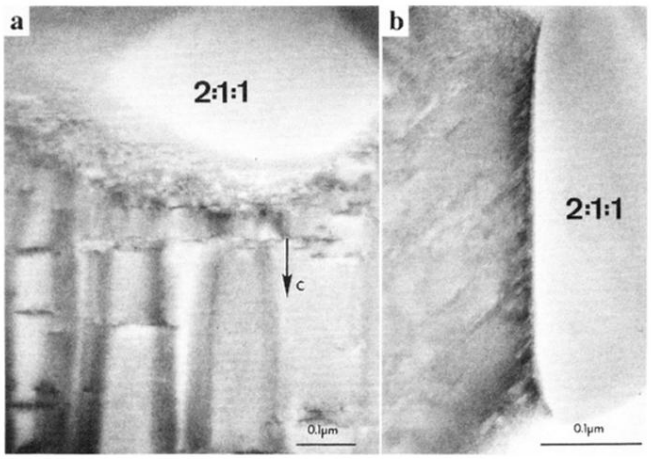

FIG. 5. TEM images of 2:1:1 inclusions in the 1:2:3 matrix viewed along [100] or [010] showing the high density distribution of stacking faults around the 2:1:1 particle interfaces.

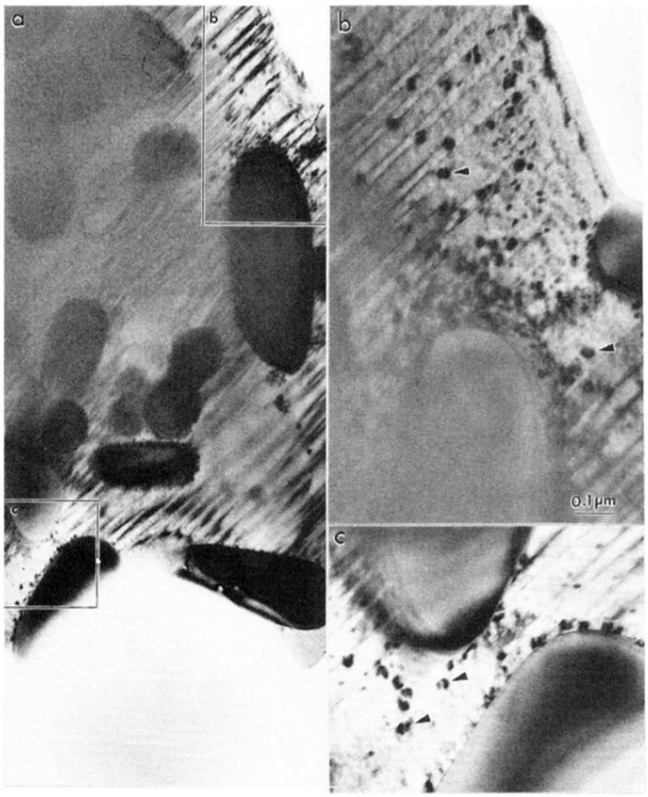

FIG. 6. TEM images of 2:1:1 inclusions in the 1:2:3 matrix viewed along [001]. (b) and (c) are enlarged images of the areas *b* and *c* indicated in (a) taken under slightly different diffracting conditions, respectively.

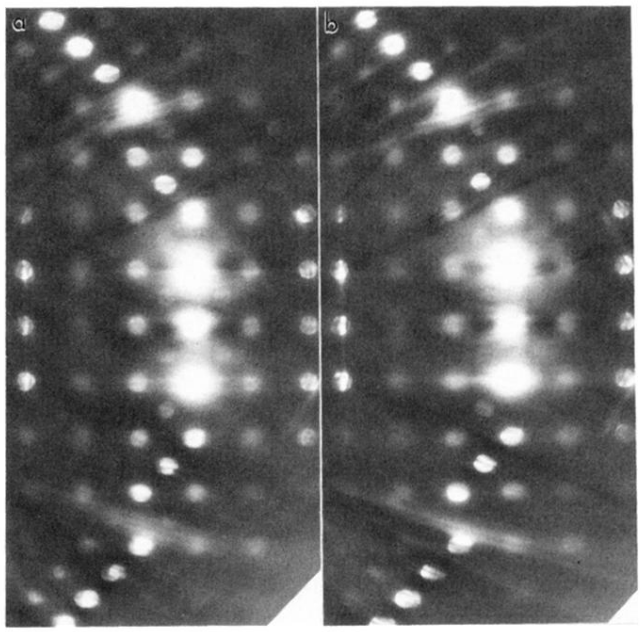

FIG. 7. (a) and (b) are CBED patterns taken using a 2-nm-diam electron probe from a dislocation loop and the 1:2:3 matrix, respectively.

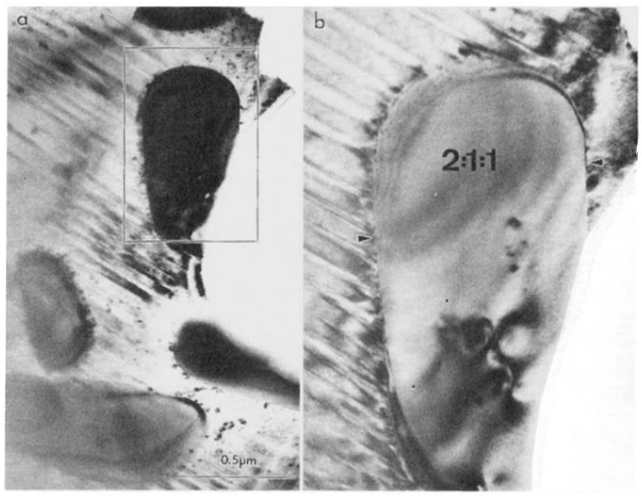

FIG. 8. TEM images of 2:1:1 inclusions in the 1:2:3 matrix viewed along [001]. (b) is an enlarged image of the area *b* indicated in (a) taken under slightly different diffracting conditions.